*PROCEEDINGS*

THE FORTY-FIFTH AND
THE FORTY-SIXTH ANNUAL

# SYMPOSIUMS
## ON THE
# ART OF SCIENTIFIC GLASSBLOWING

# 2000 & 2001


THE
AMERICAN SCIENTIFIC GLASSBLOWERS SOCIETY

*Proceedings*

*The Forty-fifth Annual*

# Symposium

on the

# Art of Scientific Glassblowing

Sponsored by
The American Scientific
Glassblowers Society

*Hyatt Resort at Lake Tahoe*
*Incline Village, Nevada*
*May 30 - June 3, 2000*

THE
AMERICAN SCIENTIFIC GLASSBLOWERS SOCIETY
*Thomasville, NC*

The American Scientific Glassblowers Society
302 Red Bud Lane
Thomasville, NC 27360
Phone: (336) 882-0174
FAX: (336) 882-0172

**Library of Congress #58-3756**

# Officers and Directors of The American Scientific Glassblowers Society 1999-2000

## Officers

| | |
|---|---|
| President | Barry W. Lafler |
| President-Elect | Doni J. Hatz |
| Secretary | Scott Bankroff |
| Treasurer | Sally Prasch |
| President Emeritus | Karl Walther |

## Sectional Directors

| | |
|---|---|
| Michael Palme | A. Ben Seal |
| Dennis Briening | Hans Rohner |
| Frank Meints | Gary T. Farlow |
| Daniel Wilt | Gene Nelson |
| Joseph S. Gregar | Gary S. Coyne |
| J. Jeffrey Babbitt | Bob Singer |
| Sean G. Adams | |

George Sites
*Director Emeritus*

James K. Merritt, Executive Secretary
Dawn Hodgkins, National Office Manager
Marylin C. Brown, Ph.D., *Fusion & Proceedings* Editor

## Past Presidents

† J. Allen Alexander
* Karl H. Walther
Arthur Dolenga
Alfred H. Walrod
Richard W. Poole
† William E. Barr
† Charles J. Cassidy
† Jonathan Seckman
William A. Gilhooley
M. Howe Smith
Billie E. Pahl
Theodore W. Bolan
Earl R. Nagle
Werner H. Haak
Gordon Good
Robert G. Campbell
† Helmut E. Drechsel
Lawrence W. Ryan, Jr.
† Joseph W. Baum
Andre W. Spaan
Donald E. Lillie
Wilbur C. Mateyka
Jerry A. Cloninger
† David Chandler
† Owen J. Kingsbury, Jr.
Raymond L. Carew
James K. Merritt
Joseph S. Gregar
Joseph Walas, Jr.
A. Ben Seal
Robert J. Ponton
Ian B. Duncanson
Allan B. Brown
Richard C. Smith
Richard P. Gerhart
David G. Daenzer

† Deceased
* President Emeritus

# 45TH SYMPOSIUM COMMITTEES

| | |
|---|---|
| General Chair | Victor Mathews<br>M-Tech Industries |
| Symposium Coordinator | Jerry Cloninger<br>Georgia Institute of Technology |
| Artistic Chairs | Tom Orr<br>Orr's Glassworks Venicia |
| | Arthur Hanner<br>Kontes/Custom Glass Shop |
| Exhibits Chair | Bill Roach<br>Wale Apparatus Co., Inc. |
| Hospitality Chairs | Tish Buti<br>Litton Engineering Labs |
| | Paul De Coux<br>Quark |
| Junior Seminars Chairs | Joseph Gregar<br>Argonne National Lab |
| | Rand LeBaron<br>Glastec |
| Marketing Chair | Ralph Joiner<br>Farlow's Scientific Glassblowing, Inc. |
| Multimedia Chair | Jim Breen<br>Kontes/Custom Glass Shop |
| Regular Member Seminars Chair | Allan Brown<br>University of Connecticut |
| Seminar Chair | Charles Litton<br>Litton Engineering Labs |
| Technical Papers & Posters Chair | Skip Huckaby<br>Orca Glaswerke, Inc. |
| Technical Workshops Chair | Gary Farlow<br>Farlow's Scientific Glassblowing, Inc. |

# CONTENTS

## Papers



## Other Information

# Papers

# Construction of a High Density $^3$He Nuclear Target Cell Made from GE 180 Aluminosilicate

**by**
**Michael J. Souza**
**Dept. of Chemistry**
**Princeton University**
**Princeton, New Jersey 08544**

Nuclear accelerators have been used for decades as a tool to investigate atomic particles. However, due to their high costs physicists can no longer assume that bigger and more powerful accelerators will be built in the near future. Nevertheless, by making significant improvement in target design, scientists can extend the lifetime of existing particle accelerator labs. In particular, spin-polarized nuclear target cells have proven to be essential instruments for providing defined and elegant targets for the field of Atomic and Nuclear Physics.

Spin-polarized atoms are used to address fundamental questions in particle physics. Precision measurements of interactions between spin-polarized atoms and external fields can reveal the properties of elementary particle interactions; the spin interactions of atoms offer a huge and rich area for study. The interaction of polarized light with atoms, of polarized atoms with each other, and of polarized atoms with surfaces, are all active areas of research. Important questions include identifying the mechanisms that cause spin relaxation as well as the means by which polarization can flow from one system to another. Research topics include the spin interactions of atoms that are in the solid state, such as xenon ice and alkali-metal hydrides. In much of this work, laser techniques are used in combination with nuclear magnetic resonance to produce powerful new experimental probes.

Experiment **E94-010,** conducted at the Thomas Jefferson National Accelerator Laboratory (TJNAF), probed the way in which quarks assemble themselves into protons and neutrons. The experiment involved the scattering of spin-polarized electrons from a spin-polarized $^3$He target at incident energies between 0.9 and 5.1 GeV. By studying the small spin-dependent asymmetries that occur in the scattering process, the researchers were able to test the "Generalized Gerasimov-Drell-Hearn (GDH) Sum Rule," a theory whose predictions depend on the spin structure of the nucleon. The degree to which the Generalized GDH Sum Rule holds sheds light on the dynamics that govern the forces between quarks and the ways in which those forces result in the protons and neutrons that we observe in ordinary matter. The heart of the experiment was a sample of polarized $^3$He contained in the glass cell that is the primary subject of this paper.

**Figure 1** Aerial View of CEBAF Accelerator

Jefferson Lab's accelerator is a racetrack-shaped machine used to make electrons travel at nearly the speed of light. Jefferson Lab's accelerator is about 1.4 kilometers around (about 7/8 of a mile) and was built in a tunnel 8 meters (about 25 feet) underground. Electrons gain energy as they pass through the straight sections of the accelerator and are steered by large electromagnets as they pass through the curved sections. An electron can travel around the accelerator as many as five times, gaining energy with each trip (as much as 6 billion volts); it is then directed to one of the three large, hill-like experimental halls where it collides with the target.

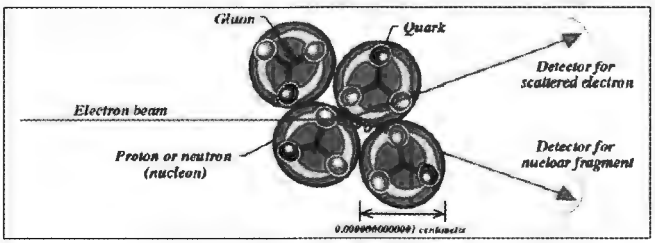


**Figure 2 Quark**

How can scientists possibly study something that small? Scientists at Jefferson Lab use electrons to study quarks. They direct a beam of electrons at a sample of matter and observe how the electrons interact with it.

To understand the problem of measuring and defining quarks, one must realize their scale. For instance, **a sheet of aluminum foil is about 250,000 atoms thick. If you took one of those atoms and enlarged it so that it was the size of the earth, a quark inside the nucleus of that atom would be no larger than your fist.**

## Material Requirement for Nuclear Target Cell

The nuclear target cell used for this experiment required a special glass consisting of the following characteristics: impermeability to helium, resistance to hot alkali metals, low ferrous content, and high dielectric properties. These characteristics are most commonly held by aluminosilicate glass. Of this type of glass, the most suitable was deemed to be GE 180 a glass made by General Electric's Lamp Division; it is most commonly used for halogen lamps.

**Comparative Data**

The properties of General Electric Type 180 aluminosilicate glass tubing compared to other materials currently used in halogen cycle lamps. (Published values, subject to normal manufacturing variations.)

| | GE Type 180 | GE Fused Quartz | CORNING Type 1724* |
|---|---|---|---|
| Softening Point °C | 1015 | 1670 | 926 |
| Anneal Point °C | 785 | 1140 | 726 |
| Strain Point °C | 735 | 1070 | 674 |
| Thermal Expansion (0-300 °C cm × $10^{-7}$/cm/cm°C | 45 | 5.5 | 44 |
| Density (gms/cc) | 2.77 | 2.20 | 2.64 |
| Total Alkali % | <.045 | <.005 | <.150 |
| Soda % | <.030 | <.002 | <.100 |
| Electrical Resistivity ($\log_{10}$ ohm) × cm | | | |
| @ 250 °C | 12.7 | 11.8 | 12.4** |
| @ 350 °C | 11.1 | 10.2 | 10.8** |
| Reboil Rating (on a scale 1-poor to 10-excellent) | 8 | 10 | 5** |

**Figure 3**
Comparative Data

In general, flame working aluminosilicate glass can be a difficult operation. There is an extreme tendency to cause a condition known as reboil in the glass. Reboil is a condition where constituent materials of the glass outgas in the fusing process. The gas is trapped in forms of bubbles in the glass and, in extreme situations, disassociation occurs and the glass breaks down. However, GE 180 material is far more resistant to this malady than most other aluminosilicate glasses. In addition, GE 180 has proven to be fairly resistant to the effects of rubidium vapor at elevated temperatures around 280c. Finally, its ferrous content seemed measurably lower than any other aluminosilicate available.[1]

[1] Ferrous content may vary in each glass type and is generally believed to be in the neighborhood of parts per thousand in Corning aluminosilicate. GE 180 is along the order of parts per 100k.

The one limiting factor in our decision to use GE 180 was the fact that the material is only available in relatively small size diameters. These sizes begin around 2mm o.d. and increase their size in one-millimeter increments. However, their largest size is limited to fairly small diameter of 16mm with a 1.2mm wall. This would normally be a significant obstacle to overcome. But due to high-pressure requirements and surface phenomena, re-blown or resized glass is a preferred condition for these cells.

A polarized cell is simply a container holding hyper-magnetized gas. How much of the gas is magnetic and how long the gas can hold its magnetic state varies from cell to cell. Generally speaking, out of a dozen or so cells made, the averages were around 50% polarization and a T1 (lifetime) of <60 hours. Past experiences had shown a remarkable improvement in cell quality. It was thought that the surface interaction of the glass and the spinning nuclei was an important factor and investigation of the glass surfaces done by AFM (atomic force microscopy) seem to indicate a smoother surface.

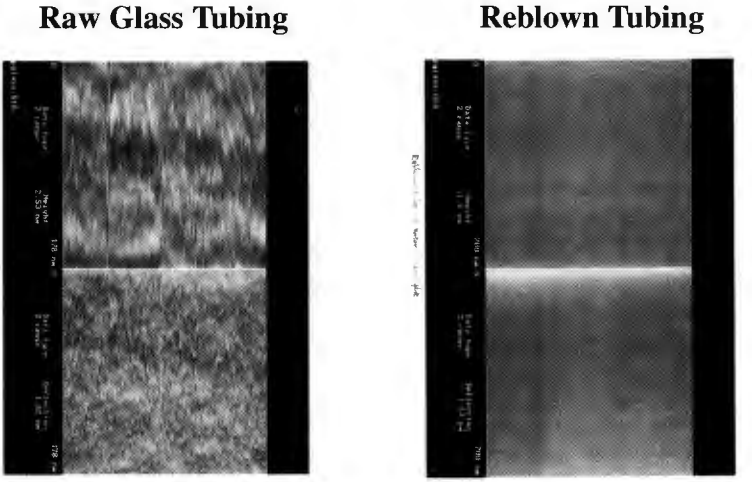


**Figure 4** AFM Scans
The scan on the left details the inner surface of a 13mm tube made from Corning 1720. To the right a section of that same tube was re-blown to 19mm and the surface measurement clearly indicates a smoother surface along the atomic scale of the glass.

## High Pressure

Due to the requirements of the experiment, the cells faced a design paradox. Physicists want to scatter as many nuclei as possible inside the cell. The glass acts as a buffer. Thus, the more glass present in front of the nuclei the less interaction will occur between the electron beam and the polarized gas. To overcome this, the cell has to have very thin entry and exits windows for the beam to pass through, and yet at the same time, as much gas as possible inside the cell. Thus, the cell is filled to 10 atmospheres pressure[2] (roughly 150 psi). To get the Rb metal inside the cell into a vapor, state the whole cell is heated to 260c. As such, the internal pressure increases to nearly 250psi.

[2] A unit of pressure equal to the air pressure at sea level, approximately equal to $1.01325 \times 10^5$ newtons per square meter.

The target windows where the electron beam enters and exits were 19mm test tube-shaped with very thin round bottoms. Each round bottom end is blown to exacting tolerances of 5.5 mils thick + or – 0.490 mils.[3]

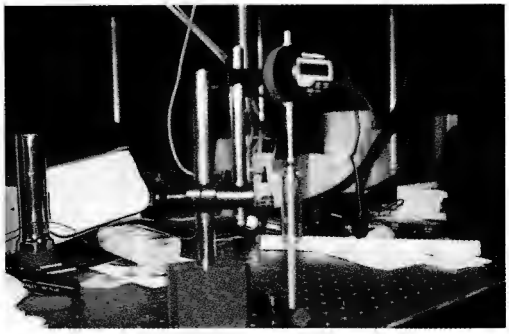

**Figure 5**

A test tube-shaped thin round bottom is made and numbered. It is placed on a brass fixture with a similar radius. Prior to this, a digital micrometer is zeroed out on the brass fixture. Once the glass is in place, the micrometer measures the displacement between the brass and the micrometer needle.

Windows are manufactured in large quantities. Each cell requires two windows and out of a run of 24 windows, perhaps as many as six are within thickness tolerances. Once a window is within specification, it has to be pressure tested to 280 psi. In this operation, over half of the windows will burst. Thus, for every successfully completed window there are nearly 10 windows produced that never make their way onto a finished cell.

**Figure 6 Pressure Testing**

Each window that falls into spec is then sealed onto ¼" kovar seals. Brass fittings are used to pressure test each window to 280 psi for 10 minutes. Under these conditions only 40% of the windows tested survive.

[3] A unit of length equal to one thousandth ($10^{-3}$) of an inch (0.0254 millimeter).

**Schematic for Cell**

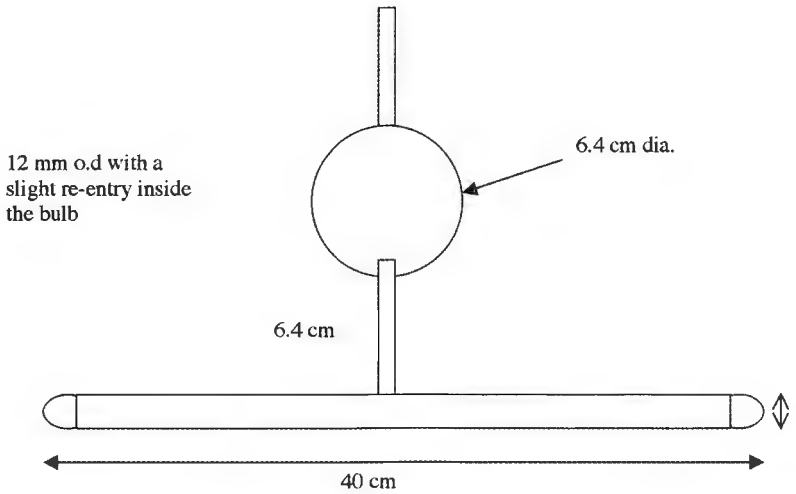


Every component of the cell was made from 15.8mm o.d. tubing with a 1.8mm wall. Prior to fabrication, appropriate sized segments were cut and soaked for five minutes in a full strength solution of nitric acid and then rinsed in deionized water.

**Figure 7 Resizing**

A graphite block is fixtured onto the fire carriage of a Litton lathe and the tube is blown to the block.

Resizing 18" long sections of 19mm o.d. tubing starts the laborious process of making windows. The same material is also used to complete the 40cm long target tube. 24" long sections are used to make the 64mm bulb (pumping chamber) and the 12mm tube connecting the bulb to the target tube.

**Figure 8 Completed Bulb**

A constriction is made on an 8mm o.d. tube above the pumping chamber and the component part is attached to the target tube via the 12mm o.d. transfer tube. As such, the cell is completed and the volume is measured by weighing the vessel when it is empty and next filling segments of the cell with deionized water and measuring the weight of the water inside the cell.

**Figure 9 Water Volumes**

Each cell is named and the values are recorded. A titanium-scribing tool also numbers every window on each cell. When applied, this leaves a permanent black colored mark near each window of the cell. Every cell is attached to a high vacuum system and pumped out in a furnace of 480c to an ultimate vacuum of at least 1x10-8. This process takes four days.

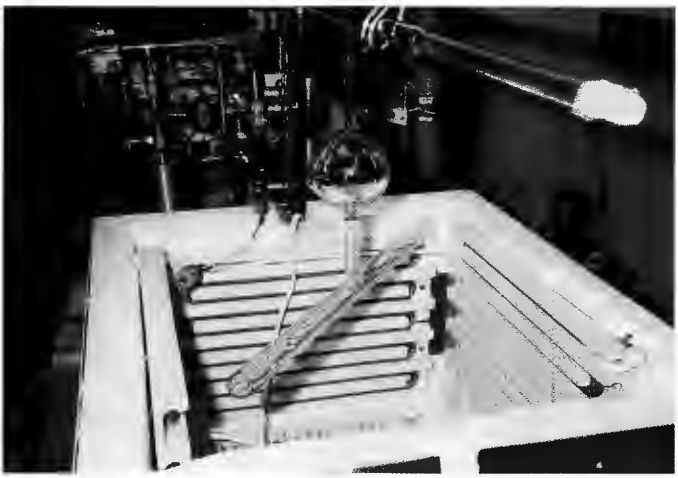

**Figure 10 Bake Out**

Open rubidium ampoules are inserted into the manifold prior to evacuation and remain sealed in the manifold outside the furnace during the four day pump-out. Afterwards, the cell is brought to room temperature and the Rb is "chased" into the pumping chamber of the cell. This is done by heating the Rb with a small torch and moving the condensing metal along the manifold and into the cell. Because the transfer tube is ring sealed to a slightly higher level within the bulb, the molten Rb is prevented from running into the target tube where it would be difficult to reheat later in the beam line.

**Figure 11 Dewar Assembly One**
A two-piece stainless steel dewar is assembled

**Figure 12 Dewar Assembly Two**

The two halves are joined by a silicone gasket with an opening on top that is sufficient enough in size to allow the transfer tube to exit the dewar.

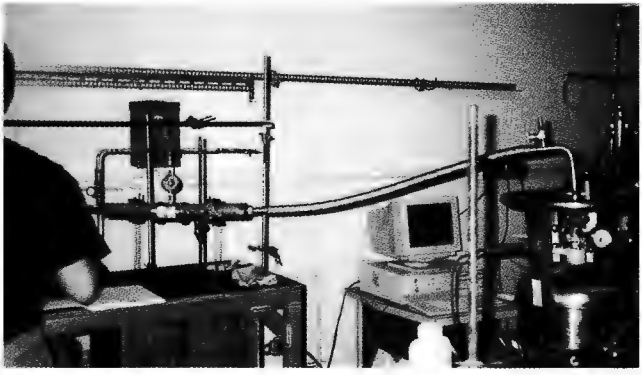

**Figure 13 Liquid Helium Set-up**

A liquid helium caddy is attached to the dewar and condenses backfilled $^3$He into a liquid.

**Figure 14 Vacuum Seal-off**

Once an appropriate amount of $^3$He is backfilled into the cell. The cryro-pumped cell is below atmospheric pressure and can be sealed-off.

With the Rb in place, a stainless steel dewar is assembled around the target tube of the cell. Liquid helium is flowed through the dewar and super cools the $^3$He that is backfilled into the cell.

The cell is finally sealed-off from the manifold in an atypical fashion. Instead of lowering the cell or dewar, the manifold itself is raised to achieve the separation of the completed cell from the vacuum system. The flexibility to lift the manifold tube is provided by a flexible stainless to glass seal where the glass manifold connects to an all-metal vacuum system.

**Figure 15 Gas Handling System**

An ultra-pure gas handling system is used to evacuate each cell and then to backfill them with 10 atmospheres of $^3$He gas.

## Conclusion

This project was deemed highly successful. The experiment included numerous collaborators from various other universities and Princeton was sole-fabricator for the cells used in the experiment. In all, over a dozen cells were fabricated and as a group these cells were the most highly-polarized cells ever made. Average polarization and T1's were among the highest ever achieved as a project for the DOE.


## Acknowledgements:

I would like to thank the collaborators on this project: Professor Gordon Cates and Graduate Student Ionnis Kominis from the Atomic Physics Group in the Physics Department at Princeton University. In addition, I would like to acknowledge the continuing support of the Chair of the Chemistry Department, Professor George McLendon.

Mr. David Warren at GE Lamp Division


## References:


Happer, W., Appelt, S., Baranga, A. Ben-Amar, Erickson, C. J., Romalis, M. and Young, A. R. "Theory of Spin-Exchange Optical Pumping of $^{3}$He and $^{129}$Xe," *Phys. Rev.* 58. Supplement A. (1998): 1412.

Romalis, M. V. and Cates, Gordon D. "Accurate $^{3}$He polarimetry using the Rb Zeeman frequency shift due to the Rb-$^{3}$He spin-exchange collisions." *Phys. Rev.* 58. Supplement A (1998): 3004.

Souza, Michael J. "Atomic Force Microscopy Scans of Glass Surfaces Used in Polarization Cells." *Proceedings of the Forty-third Symposium on the Art of Scientific Glassblowing.* (Bloomington, MN, 1998): 78-82.

Souza, Michael J. "Super Thin Windows for High Density $^{3}$He Target Cells." *Fusion* 42.4 (1995): 20-28.

# High and Low Temperature I R Cell

**by**
**Robert Ponton**
**University of Wisconsin- Milwaukee**
**Milwaukee, WI 53201**

This paper will deal with construction techniques used to produce a cell capable of working at both cryogenic temperatures as well elevated temperatures reaching 700-800 degrees centigrade. The bulk of the cell was built using borosilicate glass. The high temperature portion was constructed from fused silica. Illustration 1 shows the completed apparatus.

**Illustration 1**

This apparatus was used primarily to study various catalytic reactions on paper thin alumina sample pellets. After preparing the powdered alumina samples, the sample was pressed into a paper-thin pellet using a standard arbor press with stainless steel pellet molds. These samples are particularly fragile. We needed to develop a sample holder that would provide the maximum surface area contacting the pellet. The sample holder had to also support the alumina pellet.

**Part 1:**

Starting with the construction of the fused quartz end and sample holder, fuse a 12-inch length of 8mm quartz to a 3-inch length of 15mm quartz. Test tube the end of the 15mm and blow open an 8mm hole in the center. "T" seal a short piece of 28mm quartz. Cut the 28mm tubing to allow 1-2mm extension on each side of the 15mm. Flair a 15mm length of quartz to 28mm diameter. Cut this at 25mm long. Repeat this procedure for second arm. (Illustration 2)

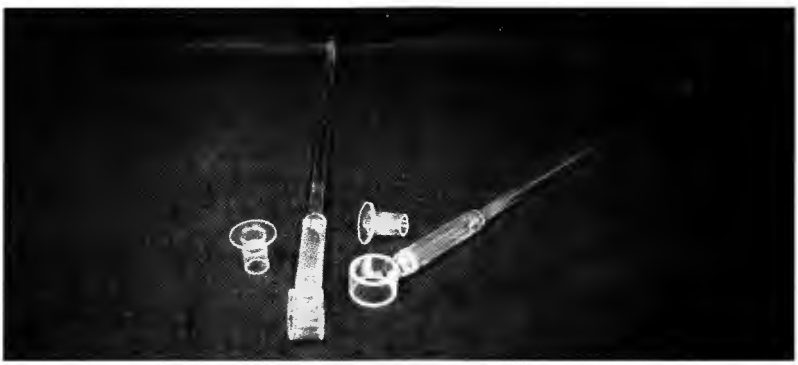

**Illustration 2**

Place the 8mm-handle portion of sample arm in a ring stand. Carefully place the 28mm-flair tube in the 28mm sample arm. With a small flame, seal the flair to the tube. Care should be exercised to make a seal with no pinholes. Repeat this procedure for second arm. (Illustration 3)

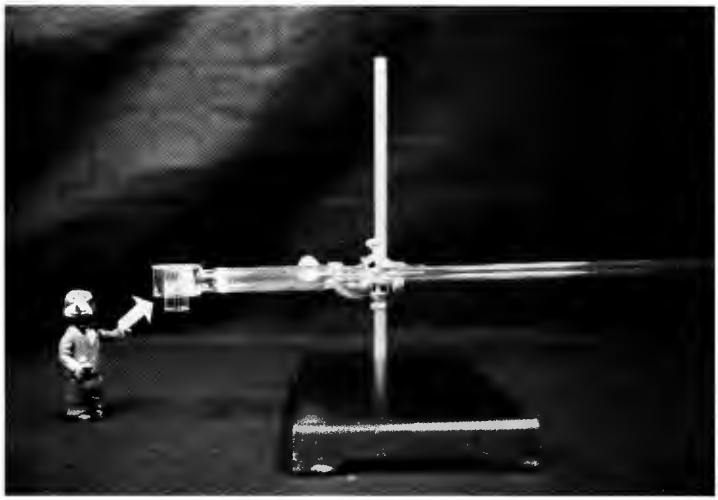

**Illustration 3**

Bend the 8mm tube to form a handle on the same axis as the inner diameter of the 15mm tubing. Connect a blow hose to the 8mm tubing. A carbon rod is turned down to the inner diameter of the 15mm and chucked in the tailstock of the lathe. This will ensure that the piece runs on center. Adjust the 8mm handle as needed. Remove the carbon-centering rod. Flair the protruding 15mm up to meet the 18mm. Seal together and flatten using a carbon paddle. Care needs to be exercised to maintain the hole diameter. Re-work the first side with a sharp flame. Repeat this procedure for the second arm. (Illustration 4)

**Illustration 4**

Remove the bent 8mm handle, retubulate with another 12-inch length of 8mm tubing. Chuck this in the headstock of the lathe and blind seal a length of 8mm from the tailstock. Elongate the bottom half to facilitate adding the nichrome wire later. Clear all the bloom leaving the 8mm handle on the bottom. Repeat this procedure for the second arm. (Illustration 5)

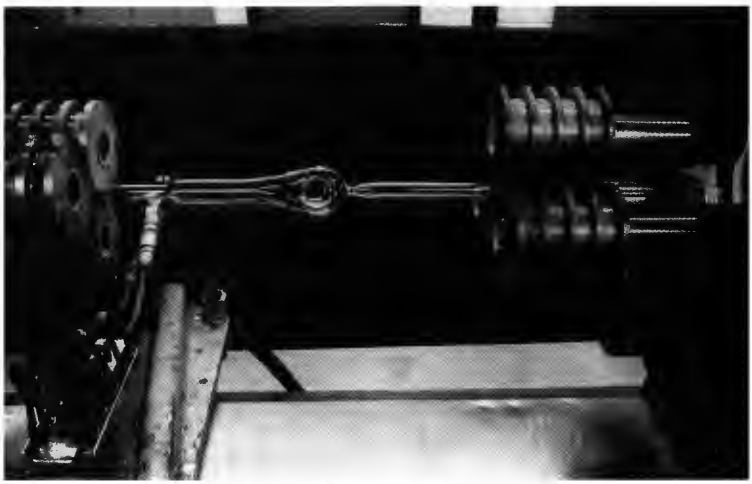

**Illustration 5**

Using a belt sander or a lapping wheel, grind one side of the sample arm flat. 600 grit silicon carbide is recommended for the final grind. Repeat this procedure for the second arm.

Fabricate quartz to borosilicate graded seal. Add a stainless steel bellows having borosilicate tubing on each end. Add this to the quartz sample arm. The second sample arm will be graded directly to borosilicate. Remove the 8mm handle from the bottom. (Illustration 6)

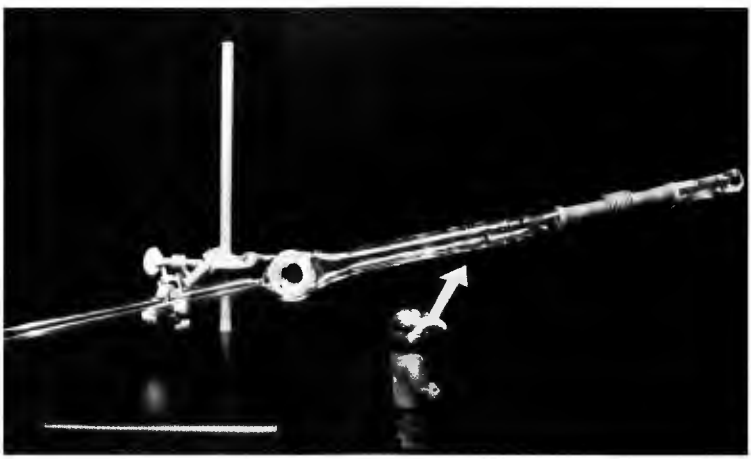

**Illustration 6**

Seal a length of 19mm standard wall tubing to the top of a 12/18 outer joint. Blow open the 19mm at 2cm above the top of the joint. Make two. These are then sealed to a short length of 38mm standard wall tubing. These arms should be parallel with a separation of 2-3mm. Add a support rod below the joints. (Illustrations 7&8)

**Illustration 7**

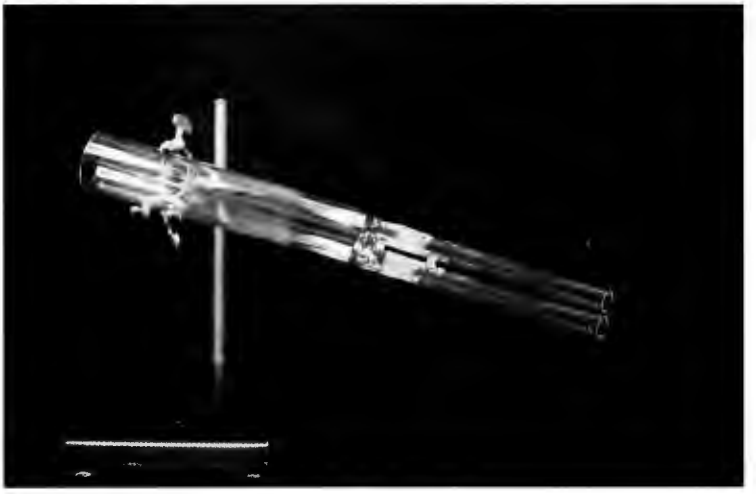

**Illustration 8**

Fire cut the 38mm standard wall tubing approximately 1.5cm above the ground joints. Flare the open end of the 38mm tubing to fit inside of the #50 O-ring joint. Pack the assembly into your holder and proceed to make the Dewar seal. Add the # 7 O-ring joint to the top of the Dewar seal. This will be used for the thermocouple attachment. (Illustrations 9&10)

**Illustration 9**

**Illustration 10**

Attach the two sample holding arms below the 12/18 standard taper joints. Make sure the two ground portions sit flush to each other and that the openings are in alignment. The completed sample section will allow for a great deal of flexibility due to the stainless steel bellows. (Illustrations 11&12)

**Illustration 11**

**Illustration 12**

Wind two nichrome wire heating coils using a number 10/18 standard machine screw. Leave sufficient wire on each side of the coil to reach above the Dewar seal. These are guided through the sample arms by attaching a magnet to one end and drawing through with a second magnet. (Illustration 13)

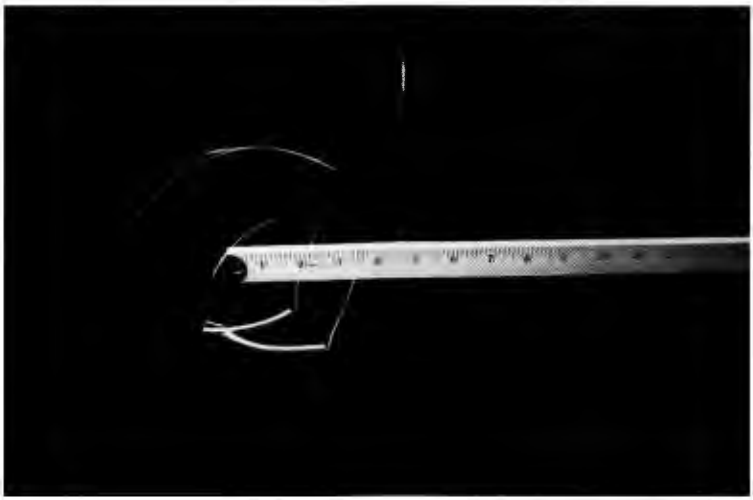

**Illustration 13**

**Part 2:**

Push up a maria approximately 2cm from the # 50 O-ring joint. Blow open a hole close to the maria and seal a length of 41mm standard wall tubing to the O-ring joint. (Illustrations 14&15)

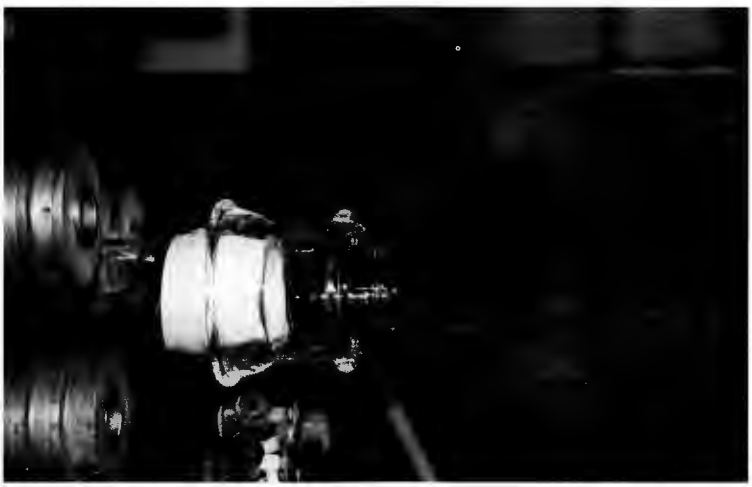

**Illustration 14**

**Illustration 15**

To determine where the windows will be located, measure down from the bottom of the # 50 O-ring joint on the sample arm to the middle of the opening on the quartz end of the sample holder. Make sure to allow for the thickness of the O-ring. Use this measurement to locate the point where the 22mm standard wall tubing will be added. Proceed to add two lengths of 22mm tubing directly opposing each other for window access and a length of 10mm standard wall tubing for a stopcock. Test tube the 41mm tubing just below the window area.

Cut and grind the 22mm and 10mm tubing so that it fits snuggly inside of a length of 75mm standard wall tubing. The 75mm tubing will make up the outer water jacket. When you have the 22mm and 10mm tubing ground to fit, chuck the assembly in the lathe using a holder on the O-ring joint. Carefully slide the 75mm tubing over the end and up to the maria. (Illustrations 16&17)

**Illustration 16**

**Illustration 17**

Starting at the bottom of the cell, warm and fuse both window openings fully to the outer jacket. Do not seal the 10mm stopcock port yet. Put a Bunsen or some type of annealing fire on this area while you work on the other end.

Warm up the 75mm and maria, paddle down the 75mm to meet the maria and work out the ring seal thoroughly. Add the top stopcock and a rod brace above the ring seal. Next, add a barbed hose connection below the ring seal. Bend the tube on the hose connection over and fuse it to the stopcock. This will allow you to blow on both sides of the ring seal while finishing the bottom. Thoroughly flame anneal this area. (Illustration 18)

**Illustration 18**

Slowly re-warm the window area back to the working temperature. Blow open the window ports and add the 20mm O-ring joints that will hold the KBR windows. Add the bottom stopcock, flame anneal. Oven anneal. (Illustration 19)

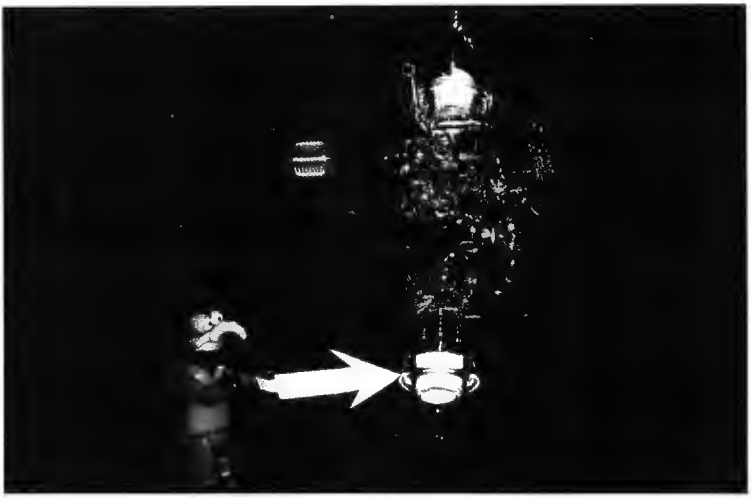

**Illustration 19**

The ground joints at the top of the sample section are for holding jacketed funnels when using liquid nitrogen to cool the sample. This cell was used primarily at elevated temperatures reaching 700-800 degrees centigrade. Viewing through the KBR window, we can see the bright glow and the nichrome wire coils. (Illustrations 20&21)

**Illustration 20**

**Illustration 21**

# Particle Inclusions in Optical Fiber Manufacturing

by
**Clifton W. Draper**‡
**Sensors Unlimited, Inc.**
**Princeton, NJ 08540**

Abstract: Certain kinds of particle inclusions in synthetic silica glass can produce low strength failures in optical fiber during proof testing. This paper presents a very general overview of the origins of particles causing these kinds of failures in production environments. One family is refractory particles introduced into the factory as a result of the need to achieve extremely high temperatures for fiber drawing. A second are those produced by the conversion of metallic steel particles into chromium oxide particles. Another inclusion is crystobalite, formed when surface devitrification of the fiber occurs during the last stage of fiber production. Since optical fiber manufacturing has much in common with fused quartz production the topic is likely to be of general interest to Society membership.

## 1. Introduction

The manufacturing of optical fiber for use in telecommunications, internet traffic and cable TV transport is a fairly mature industry. Corning Incorporated and Lucent Technologies dominate fiber manufacturing. This is especially true for the most recent fiber designs tailored to meet the demanding dispersion requirements of dense wavelength division multiplexing. Optical fiber is basically a commodity selling for literally pennies a meter. Although non-silica fibers have niche markets, nearly all optical fibers are basically pure synthetic silica of 125 micrometer diameter that contain a central "core" region that has a modified chemistry. The silica fiber is coated with one or more polymer layers that bring the final fiber diameter to 250 micrometers. For those who have never handled or seen a strand of optical fiber, it has roughly the feel and appearance of a stiff piece of thin-gauge fishing line. The most common "dopants" used to alter the refractive index properties of the central core include germanium, phosphorus and fluorine. A number of different manufacturing processes are in use today. These include modified chemical-vapor deposition (MCVD), outside vapor-phase deposition (OVD) and vapor-phase axial deposition (VAD). All of these manufacturing processes end up producing a long cylindrical piece of glass referred to in this industry as a "preform." Preforms are placed in draw furnaces where the glass is heated to temperatures greater than 2000 degrees Centigrade. The glass becomes sufficiently soft and fiber is drawn at high velocity. A detailed understanding of the manufacturing processes used to produce preforms is not needed to appreciate the detrimental role particle inclusions play; however a basic understanding is useful.

The drawing of preforms involves: positioning of the glass cylinder above the furnace opening, lowering the preform to form a "drop,"[1] aligning the fiber in the coating cup, stringing of the fiber onto take-up spools, ramping up to the target equilibrium draw velocity, and finally, transferring to a product spool. Typical draw velocities are in excess

‡ formerly of Lucent Technologies, Inc. 2000 NE Expressway, Norcross, GA 30071

[1] A drop can be seen on the cover of the October, 1986 issue of *Scientific American.*

of 10 meters per second. If the fiber breaks during the draw, a considerable quantity of fiber and production time can be wasted. Another significant and negative impact is the degree to which costs downstream of fiber draw are a function of the number of spools of fiber produced by draw. Obviously, an inventory of fewer full spools of fiber is preferred to an inventory made up of far more spools containing a greater diversity of fiber length per spool. Thus fiber breaks are an important yield issue. In twenty-five years of fiber production, the primary function of proof test break collection and fiber fractography have been to identify and eliminate (reduce) the incidence of breaks. We will see below that the physical location of the break causing flaw sometimes points to deficiencies in manufacturing steps that precede fiber drawing. In the case of the MCVD process, starting tubes of synthetic silica are mounted on lathes where torches provide external heating. Ultra-pure chemical mixtures flow through the tube interior. The torch moves back and forth along the length of the tube making multiple "passes." The radial glass chemistry is adjusted by varying the flow rates of silicon and germanium tetrachloride chemical sources. The hole within the starting tube is collapsed so that a solid rod is produced. This rod is overclad or jacketed with one or more additional tubes to build up the synthetic silica cladding. Such rod-in-tube processing (also referred to as jacketing) significantly increases the length of fiber that can be produced from a single preform. Both the OVD and VAD manufacturing processes also rely on "overcladding" in order to gain from the economy of increased preform size and very high draw speeds.

The screening out of defective (weak) sections of fiber is accomplished by proof testing. This may be done either on-line during the fiber drawing or as a separate process following draw. Counting the incidence (frequency) of proof test breaks is easily automated; however collecting break samples for failure mode analysis is not so easily accomplished in real manufacturing environments. As a result, one normally has a very accurate measure of production break rates, but a very sketchy explanation as to why variations take place. The basic analytical tools used in fiber failure mode analysis are the optical and scanning electron microscope. An excellent review of this subject was written by Chandan, Parker and Kalish, and published as a chapter in the text Fractography of Glass, edited by Brandt and Tressler. In an ideal situation, the proof test break sample is examined optically with the coating in place, then with the coating removed (typically a hot sulfuric acid dip). A subset of these samples may then be prepared for introduction into a scanning electron microscope. Fibers are routinely examined both "end-on" and "longitudinally" along the fiber surface nearest the fracture. With some regularity, this kind of failure mode analysis can assign the flaw producing the break to a "location" and "*cause*." For example, when examining a coated fiber end-on in the optical microscope, a bright mirror may be evident at the periphery of the glass fiber surface. The coating itself appears to be perfectly normal. After stripping away the coating and examining the fiber again at higher magnification, it is evident that a very small particle is present on the surface of the fiber and that the mirror on the fracture surface is centered on this particle, while hackle lines point to the particle. An example of such a fiber failure is pictured in the optical micrograph of Figure 1. It is clear that the flaw producing this break is a surface particle. Logical location categories include: coating, fiber surface or internal. Typical cause categories include: particle, abrasion, airline (elongated bubble) and unknown. The use of X-ray elemental analysis within the scanning electron microscope can further elucidate the

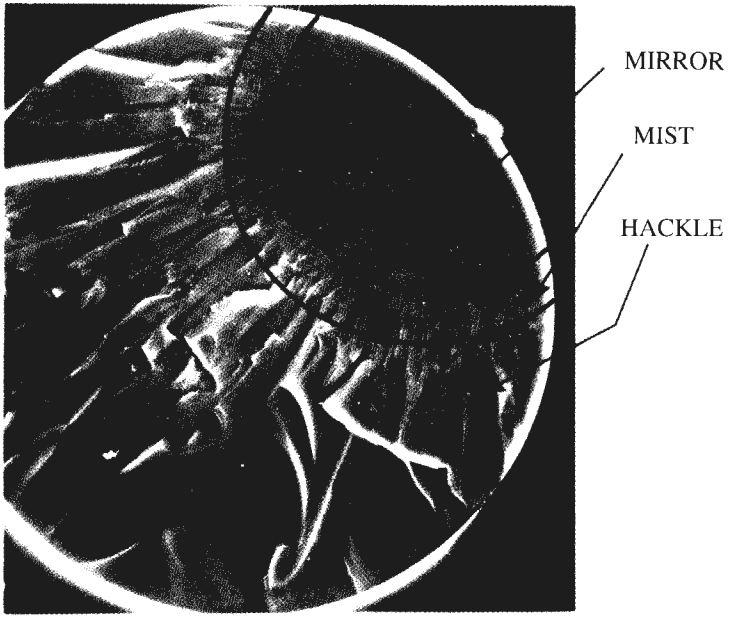


**Figure 1.** Typical fracture surface for a low strength optical fiber break. The coating has been removed. Three distinct regions (mirror, mist and hackle) are noted. The hackle lines point to the flaw causing the break, in this case a zirconia surface particle.

composition of particles. Typical electron microscopy X-ray analysis indicates that the most commonly occurring particles contain Zr-Y, Zr, Si-C, C, Cr or Cr-Fe. Although particle compositional information is available from X-ray EDS within the scanning electron microscope, this method provides no information about particle microstructure. The Raman microprobe is ideally suited for obtaining this information. In Raman spectroscopy, inelastically scattered laser light is collected from the particle. The probing laser beam is focused on the particle using a conventional light microscope. The inherent "targeting" of the particle by both hackle lines and fracture mirrors make locating the particle fairly straightforward. The wavelength of a portion of the light scattered from the particle is "shifted" in frequency by an amount characteristic of the bonding of the elements within the particle. The microstructure of the particle can be readily determined in this way since the Raman frequencies of most molecules and crystalline particles of interest are already documented in the literature.

## 2. Intentional Contamination

Fiber production is generally quantified in terms of megameters of fiber. For the purpose of a simple illustration, consider a draw velocity of 10 meters per second and a break frequency of 10 per fiber megameter (both numbers being reasonable). Then 1 million meters of fiber (roughly the distance from Atlanta to Philadelphia) would take $10^5$ seconds/60x60 = 28 hours of draw time to produce, and would contain 10 low strength failures that would be screened out by proof testing. Assuming 50% of these failures could be collected and used for failure mode analysis, we would have a sampling rate

of roughly one every five hours. Although this rate could easily be increased by collecting samples across multiple draw towers, eventually all the samples have to pass through an individual or individuals at the microscope where fiber samples are handled and examined individually. Factory sampling, failure mode analysis, is a time consuming and labor intensive effort. A radically alternative approach is that of intentional contamination. Basically, a well-characterized dispersion of particles is prepared and used to intentionally contaminate the preform. Now a single preform may yield fiber containing weak points every meter. The intentional contamination *methodology* offers a number of other advantages. These include an exact knowledge of the form of the contamination introduced as well as knowledge of the processing step and physical location where the contamination is introduced. It is easy to produce a modest inventory of ready-to-fail fiber from a single experiment. When fiber breaks occur in production, the fiber end whipping around the collection spool is often further damaged and of no use for failure mode analysis. Non-prooftested, intentionally contaminated fiber can always yield "both ends" of the fiber failure. When fiber breaks produced intentionally exactly match a category of breaks found in normal production, one has confidence that the true root cause has been identified.

The dimensions of particles that cause production breaks are typically 0.5 - 5 micrometers. It is important that the physical size of the particles contained in any intentional contamination source reflect the reality of the particle size distribution found in production samples. Commercially available powders for some particles of potential interest do exist. In a number of important cases though, the only available formulation path is to produce them from much larger "bulk" samples. This can be accomplished using a process known as ball milling. The details of how this is accomplished are not important. For the purpose of this paper, the reader should simply accept the fact that with patience and care a well-characterized and narrow distribution of particles can readily be prepared. Table 1 is a summary of the Cr to Fe X-ray ratio (as determined in the scanning electron microscope) for a collection of particles ranging in size from sub-micrometer to about 8 micrometers in diameter.

**Table 1.** Average chromium to iron peak intensity ratios determined from EDS X-ray analysis for 75 ball-milled stainless steel 316 particles used as an intentional contamination source. The ratio calculated from 316 stainless steel composition specifications is 0.26.

| | Cr/Fe | | |
|---|---|---|---|
| Particle size (micrometer) | 1 | 3 | 5 |
| X-ray peak ratio | 0.237 | 0.271 | 0.264 |
| STD (2 sigma) | 0.046 | 0.023 | 0.045 |
| | | | |
| Mean of 75 particles | | **0.257** | |
| 75 particle STD | | **0.042** | |

Stainless steel particle dispersions are applied on either the o.d. of a rod or i.d. of a jacketing tube prior to the insertion of the rod into the tube. As the methanol evaporates, the cylindrical glass body is slowly rotated and tilted so as to leave a surface deposit of fine particles. The jacketed rod is thermally treated (a graphite furnace, plasma or oxy-hydrogen torch are commonly used) while a vacuum is pulled on the gap between the rod and jacketing tube. This collapsed structure becomes the preform passed over to fiber drawing. By adjusting the number density of particles dispersed in the methanol carrier one can readily create silica fiber with particle inclusions every meter of length.

## 3. Classes of Fiber Breaks

### 3.1 Refractory Furnace Particles

Graphite resistance and stabilized-zirconia induction furnaces are basically the only two kinds of furnaces used in the drawing of optical fiber from preforms. Those interested in the details should see the chapter written by F. V. DiMarcello, C. R. Kurkjian and J. C. Williams, "Fiber Drawing and Strength Properties," in Optical Fiber Communications, Vol. 1 (Edited by T. Li, New York: Academic Press, 1985). These heat sources need to operate continuously at temperatures between 1,950 and 2,250 degrees Centigrade. Refractory materials are obviously going to be in very close proximity to the silica preform. When particles are "released" from various parts of these furnaces, they may impinge on the glass surface. The airflow existing inside these furnaces as well as within the draw towers themselves is controlled in order to minimize such particle impingement, but some number of refractory particles will contact the glass surface during fiber drawing. Figure 1 is an example of such a surface refractory particle. In this case a zirconia particle. Notice that a mirror surrounds the particle and that hackle ridges literally point at the particle causing the fiber break. Determining the origin of these particles is "a no-brainer." The particles contain the elements characteristic of the draw furnaces' themselves. That furnaces will shed particles over their useful life is a certainty. Why the frequency of breaks of the kind pictured in Figure 1 change from furnace to furnace, day to day, or "with the direction of the prevailing wind" is what makes "break free" fiber production challenging.

### 3.2 Steel Particles

Steel particles, prepared and applied to the glass as described above in section 2, produce very low strength fiber. A scanning electron microscope image of a typical fracture surface from a low strength fiber break induced by a stainless steel particle is presented in Figure 2. The mirror surrounds the particle and the hackle ridges "literally point at" the particle causing the break. This "bull's eye" pattern makes locating the micrometer-sized particle much more straightforward than would be the case without it. Locating a micrometer particle in a large silica field-of-view without the aid of these features would make the Raman microprobe very frustrating. The "look here" nature of the mirror and hackle ridges makes these instrument set-up times far more manageable.

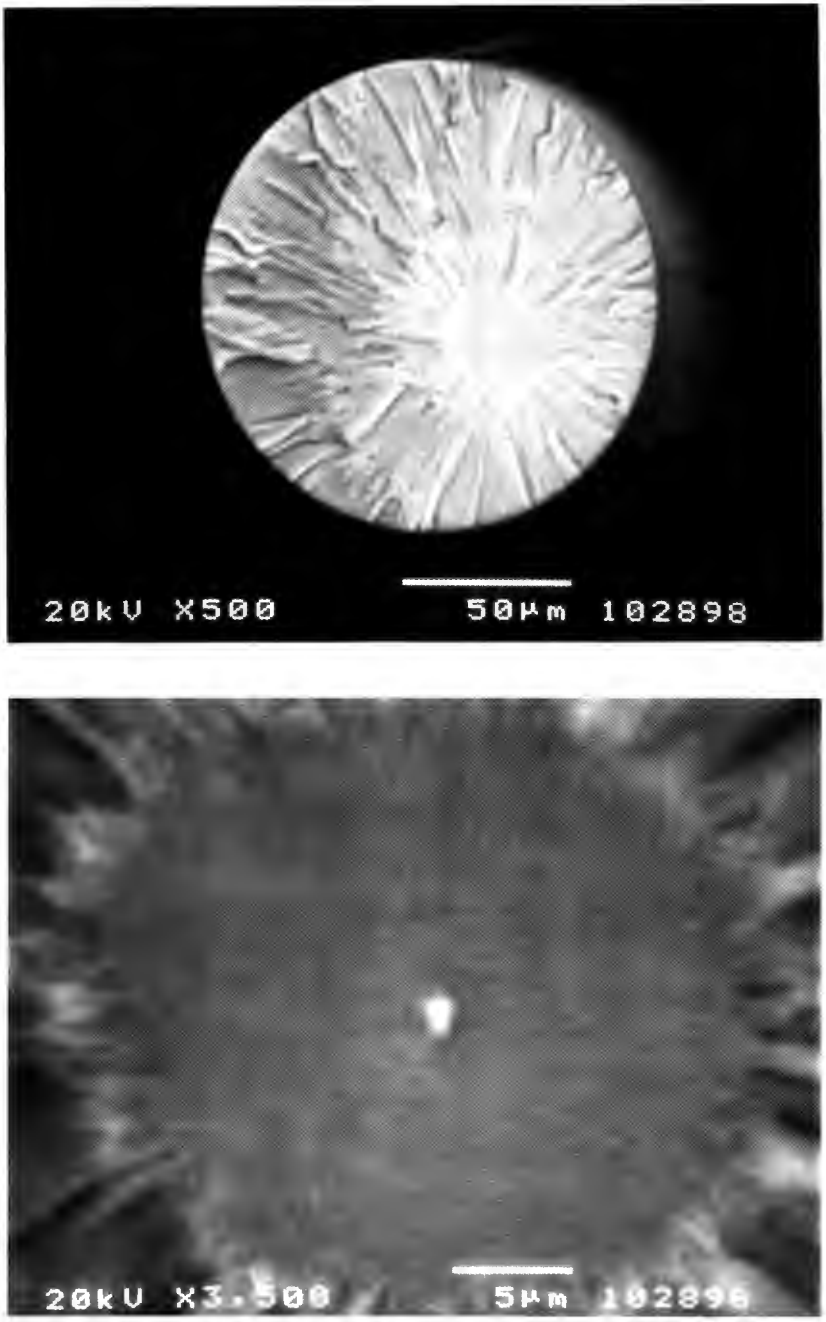


**Figure 2.** Scanning electron micrograph of fiber break caused by inclusion of stainless steel particles during the overcladding process. The distance of the particle on the "chord" running through the fiber center to the periphery is consistent with the internal rod outer diameter and distinguishes the "location" as an "interface" particle.

Figure 3 contains typical elemental analyses for two stainless steel particle induced fiber breaks. The Fe and Cr channels utilized for integrating the counts over the 100 second collection time are differentiated with shading relative to the background. For the particle in Figure 3A, the Cr/Fe peak ratio is 3.2 and for that in 3B the ratio exceeds 50. Since the starting particle ratio is roughly 0.25, this means the Fe content has decreased by a factor of about 13 in one case and >200 in the other. In many fiber samples, the Fe content has dropped so low as to be difficult to isolate from the signal noise.

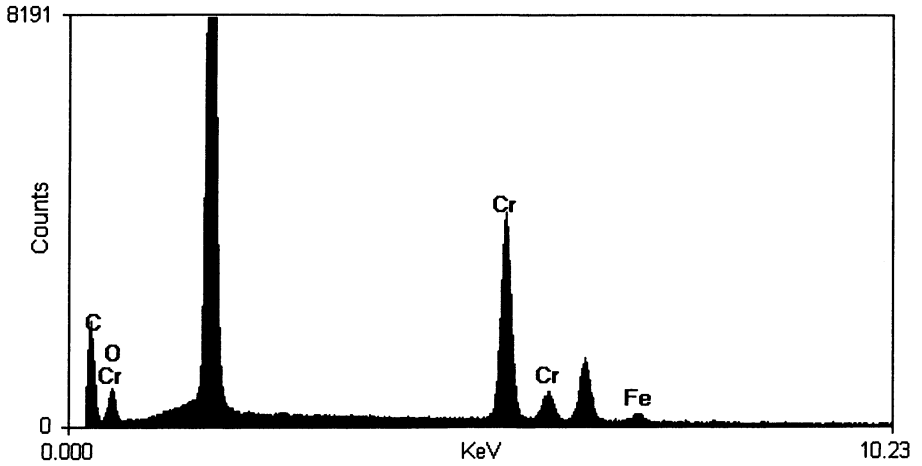


**Figure 3A**

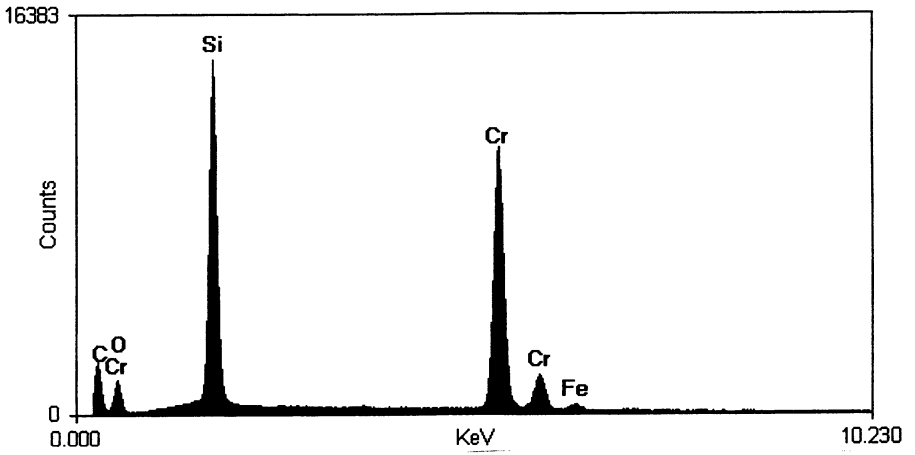


**Figure 3B**

**Figure 3.** Energy dispersive X-ray spectra typical of particles causing fiber proof test breaks in preforms intentionally contaminated with stainless steel particles. The spectra are also equivalent with a subset of normal factory production breaks. They are typically referred to as either Cr (Figure 3B) or Cr-Fe (Figure 3A) particles. In our work we measure and compare the Cr/Fe intensity ratio with that of the starting particles.

The optical and scanning electron microscopes basically provide the following information on fiber break particles: an estimate of the particle size, the mirror diameter, the particle morphology and the major elements it is composed of. No microstructure determination can be made from either of these imaging techniques. In order to understand the microstructure of the particles causing the fiber breaks, when stainless steel particles were used to intentionally produce fiber breaks, we randomly selected large numbers of fiber break samples. We also analyzed a significant number of normal factory production breaks.

The number of Cr or Cr-Fe fiber break samples (from both intentionally contaminated preforms and normal factory production) analyzed by Raman microprobe exceeded 75 in number. In every case, the particle causing the break was found to have either the cubic (spinel) $Fe_{3-X}Cr_XO_4$ or rhombohedral (corundrum) $Fe_{2-X}Cr_XO_3$ microstructure. In all cases the particles causing fiber breaks have been converted from metallic stainless steel to metal oxides primarily containing chromium, but in some cases a small amount of residual iron. In plain language, metal particles that are mostly iron go in, but chromium oxide particles are formed and end up causing the fiber failure.

### 3.3 Crystalline Silica

All glassblowers who work with or around fused quartz know that devitrification is a real possibility. Given sufficient time within just the right elevated-temperature range, crystallization is inevitable. Surface nucleation will likely play a role and so surface cleanliness of the silica is important. Many fiber breaks that are characterized by optical and scanning electron microscopy alone are classified as "unknown" when no particle or apparent mechanical damage is evident at the flaw origin, but it is obvious that a surface defect of some kind must have induced the break. In the SEM the only elemental peaks present are those of silicon and oxygen, the elements comprising the fiber itself. With the aid of the Raman microprobe, we have shown that many such fiber breaks are the result of minute regions of cristobalite having formed on the fiber surface. Since the temperature of the preform inside the draw furnace greatly exceeds the melting point of crystalline silica, these minute regions must form during the cooling down of the fiber during its last stages of elongation and transit to spooling. It is easy to imagine how local minute regions of a preform could come to be contaminated in a factory production environment making that part of the preform more susceptible to such a class of fiber breaks.

## 4. Discussion

Refractory inclusions are of particular concern in optical fiber manufacturing. In simple language, they do not go away and the mismatch between their physical properties and the surrounding silica matrix makes them the kind of flaws that consistently produce strength failures. Chromium oxide is a good example. If one examines the phase diagram for the chromium oxide – silicon dioxide system, one finds that not only are they not miscible in the solid phase, but they are not miscible in the molten state either. There is no driving force for a particle of chromia to be dissolved into molten silica even if both existed as liquids! A metallurgist might say,

"Do all the beating and heating you want, it won't make any difference."

Fiber production in real factories faces the following general kinds of challenges. To achieve the kinds of temperatures needed to draw highly pure silica, you require furnaces made of refractory materials. With time they will shed some number of particles. The most common material used to fabricate equipment and many structures inside factories is steel. Particle erosion and moving parts go hand in hand. These "background" factory particles will eventually make their way into the product itself. During elevated temperature processing, they undergo transformation from metallic to oxide particles, primarily of chromia. Building and equipping a factory without widespread use of steel is not very practical. General cleanliness may not be enough. The same applies to the root cause for divitrification. It is well understood that silica impurities drastically increase the risk of devitrification by increasing the nucleation rate. General good housekeeping practices may not be sufficient. A cleanliness paranoia may be needed to achieve and maintain optimal manufacturing efficiency.

# A Temperature Controlled Spray Chamber for ICP Instruments

by
**Patrick F. Smythe**
**Precision Glassblowing of Colorado**
**Aurora, CO 80013-1212**

**Abstract:**

This paper outlines the construction of one spray chamber design. There are dozens of designs to accommodate a wide variety of sample nebulizers, ICP instruments, and desired resulting sensitivities. This particular spray chamber is a Scott double-pass type. It has a water jacket around the main body and a vacuum jacket around both. The product is finished when it is silvered, evacuated, and tipped off.

**Introduction:**

Inductively Coupled Plasma (ICP) technology gained popularity in the mid 1970's for the multi-element capabilities over standard AA instruments. The plasma is created by means of a copper RF coil placed around the top of a quartz "plasma torch". The radio frequency is customarily either 27 MHz or 40 MHz with the power ranging from 1.0 kW for aqueous solutions to 1.5 kW for organics. The RF oscillation of the current causes RF electric and magnetic fields within the torch and a spark causes some electrons to be stripped from their argon atoms. Caught and accelerated by the magnetic field, the coil adds more energy to the electrons. This is inductive coupling. These electrons in turn strip more atoms and this ionization of the argon breaks down the gas into a plasma, forming an inductively coupled plasma (ICP) discharge.[1] Argon flowing inside the torch creates a coolant sheath around the plasma, which burns at about 10,000 degrees Celsius.

Once the plasma is stabilized, a sample (water, soil, etc.) is nebulized into an aerosol, again using argon as a carrier gas, by one of the many different nebulizers available. The resulting cloud passes through a spray chamber with the heavier droplets falling away and drained from the chamber. Another purpose of the spray chamber is to take out the pulsations associated with peristaltic pumps. The sample aerosol flows into the plasma torch through a center tip and into the plasma. The resulting burn creates a light that is analyzed by photometers and sensors for chemical content. Some instruments analyze one element at a time (sequential) and others read up to 30 elements at a time (simultaneous). There are many uses for this type of instrument. For example, there is a scientist who analyzes orange juice for the state of Florida; he can tell, through spectroscopic analysis, where the oranges were grown, so when the container says "100% pure Florida Orange Juice," it is just that.

1 Charles B. Boss and Kenneth J. Fredeen. Concepts, Instrumentation, and Techniques in Inductively Coupled Plasma Atomic Emission Spectrometry. The Perkin-Elmer Corporation, 1989.

This spray chamber gives the instrument operator strict control of the chamber's internal temperature. Many organic solutions have a low vapor point and cooling the spray chamber ensures that the sample remains in its liquid state during sample introduction.

**Construction:**

It is a good idea to study the drawing prior to making any apparatus. Make the necessary calculations in order to better create the piece your customer expects. Many drawings are made by drafters and they understandably do not know what dimensional allowances are needed to fabricate a piece from glass.

This spray chamber is made with Pyrex 7740 glass. Following are the materials needed to fabricate this spray chamber:

| Qty | Material |
|---|---|
| 1 | 12/5 socket |
| 2 | Std. 5-ring hose connector |
| ~8" | 1/4" med. wall or 6mm std. wall tubing |
| 4" | 3/8" (9.5mm) heavy wall tubing |
| 6" | 5/8" (15.9mm) med. wall tubing |
| 8" | 20mm std. wall tubing |
| 8" | 35mm std. wall tubing |
| 6" | 35mm std. wall tubing (scrap piece for holding the chamber during construction) |
| 10"-12" | 48mm std wall tubing |
| 10"-12" | 64mm std wall tubing |

**Tools:**

small graphite paddle
glass blowhose "T"
1/4" graphite rod
6mm Pyrex rod
digital calipers
3 National hand torches #'s 3, 4, and 5 tips
small rosebud tip
our "robo-tip" with two #2 tips attached
bunsen burner

(These are the tools I used. They are by no means the only ones to use; use the tools you are most comfortable with.)

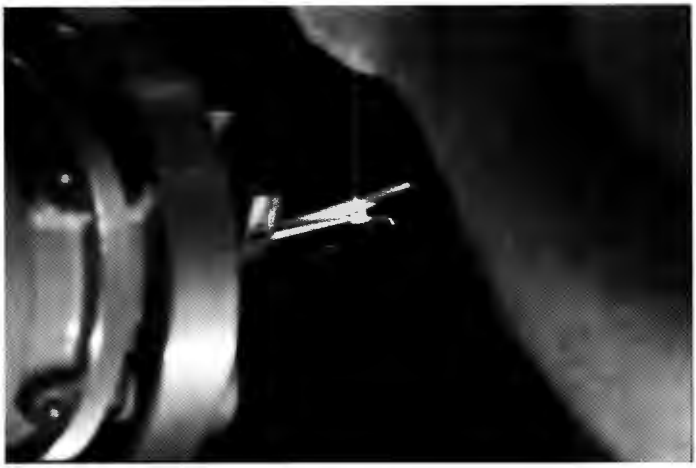

**Photo 1**

**Photo 2**

**Sub-assembly parts:**

With the 20mm tubing, produce a taper 30mm long with an i.d. of 10mm at the end. Saw the piece to an overall length of 150mm. Attach 6mm rod supports at 60mm and 130mm from the nozzle end (Photo 1). Measure the rods to ensure a height of 6mm to 6¼mm (Photo 2). The actual gap between the 20mm and the i.d. of the 35mm is 5.5mm. I found that adding a small amount of material to the supports creates a smooth attachment to the 35mm. Put a pour spout on the open end 90 degrees counter-clockwise to the support rods when viewed from that end (Photo 3).

**Photo 3**

To make the large hose connector to accommodate a 5/8" i.d. drain tube, taper a small section of the 5/8" medium wall. Push 5 rings up against each other, each one decreasing in size from the one before. Paddle each ring angling toward the next smallest with the middle ring measuring about 16mm (Photo 4). Cut to 26mm, but leave a length on the end for a handle.

**Photo 4**

Next, take the standard 5-ring hose connectors and close off the scrap ends (Photo 5). If they are the double connectors, pull them apart. With your glass knife, scratch the hose connectors at the top of the rings but do not break them apart yet.

**Photo 5**

**Photo 6**

Pull off the 48mm and the 64mm tubes to eliminate any cracking marks and to give a nice smooth edge for ring sealing (Photos 6&7). Round the 35mm and mark it at 165mm from the round end (Photo 8).

**Photo 7**

**Photo 8**

**Assembly:**

At this point I place all the pieces, holders, torch tips and anything I will use in the order I will use them on a roll around cart (Photo 9). "T" the blow hose. Fold one leg of the blowhose and hold it with a rubber band on one arm of a planetary chuck. Once this is done, begin the assembly.

**Photo 9**

Place the nozzle inside the 35mm and line up the tapered end with the mark. Erase the mark and, without moving the lathe, heat the 35mm taking care not to heat too much to avoid sticking the nozzle as it lies. After heating the main body, concentrate the heat on the support rods, sticking both to the inner wall. Once stuck, move the lathe and, through intermittent heating of the support rods, sag the nozzle to be concentric with the 35mm body. When centered, allow enough time to harden and hold the position. Turn the piece to point the support rods down. Work one support until it flows in. Turn the lathe on and, with a hot bushy flame, heat the remaining rod while the finished one is hardening (Photo 10). Work the second one and adjust the nozzle position if necessary. Flame anneal now and from here on out as needed. Use the bunsen burner to keep it hot throughout the construction.

**Photo 10**

Chuck the piece in the tail stock with a piece of carbon tape between the glass and the chuck jaws. Place your extra piece of 35mm tubing in the head stock and attach the two together. Before releasing the tail stock, push a maria at 135mm from the round end. Blow a small bubble opposite the nozzle supports, offset and tangent to the upper sidewall of the nozzle (with the round end to your right), and 110mm from the round end. This will be the sample exit with the 12/5 socket later. Blow a larger bubble above the spout on the nozzle (Photo 11). Remove excess glass and blow the bubble again. Pop a tiny hole in the small bubble, then pop a hole in the larger bubble and work them both back. Remove any excess to attain the height needed to pass the 48mm jacket over the whole body without scratching the inner wall.

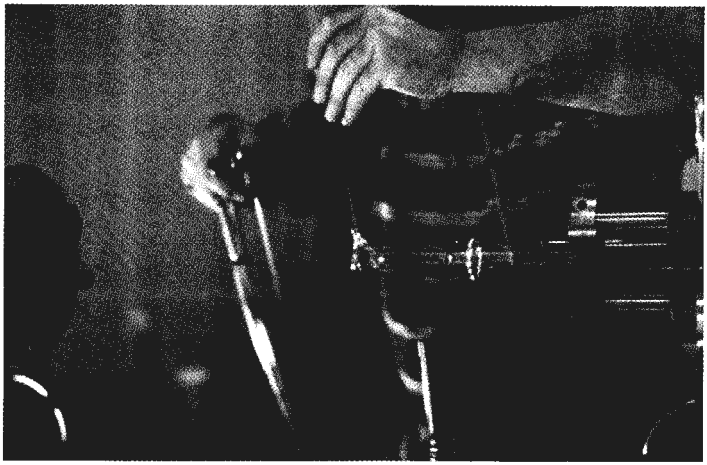

**Photo 11**

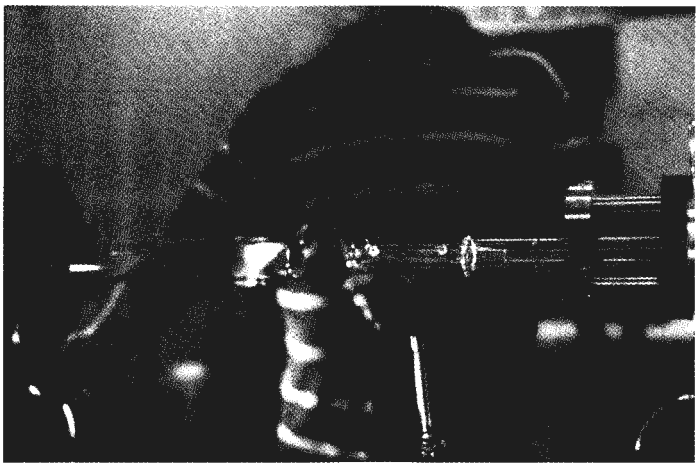

**Photo 12**

Heat the 48mm prior to passing it over the body (Photo 12). Tack the glass on the maria and allow to cool just enough to prevent sagging. Stop the lathe, heat the outer wall, and stick the sidewall to the sample exit tube near the main ring seal (Photo 13). Turn the piece over and finish the sidearm seal. Finish the main seal (Photo 14). The sidearm seal will prevent the piece from flopping around. Blow a maria on the ring seal for later. Round off the jacket (Photo 15).

**Photo 13**

**Photo 14**

**Photo 15**

With the nozzle supports facing up, blow two bubbles for the water jacket hose connector ring seals (Photo 16). When viewing from the top, the one nearest you is by the main ring seal and the other is 99mm from the first on the other side of the supports. Pop both bubbles and open up the holes to get the shape needed.

**Photo 16**

Heat the glass above the drain hole and allow it to sag until well sealed (Photo 17). Turn the piece over and finish the seal not allowing the size to decrease any. Turn the piece to bring the seal to the top and heat enough of the glass inside the ring to pull out and open the ring up a little. Blow a good bubble to raise the glass as high as possible without popping it yet.

**Photo 17**

**Photo 18**

Heat the small ring seal near the main seal and expand the hole a little (Photo 18). There is not enough glass to span the gap between the water and the vacuum jackets. Heat a piece of 6mm rod very hot and, while heating the small seal, set the rod on the seal and blow. Pull up while controlling the blow to create a "tube". This is easier than splicing a tube onto the seal. Blow a bubble and pop a small hole. Pop the larger bubble and open up both holes (Photo 19).

**Photo 19**

**Photo 20**

Adjust the height of all four openings so there will be no scratches on the next jacket (Photo 20). Heat the 64mm tube and roll it over the body (Photo 21). Tack the main ring seal and seal the small sample exit seal in the same manner as before (Photos 22 & 23).

**Photo 21**

**Photo 22**

**Photo 23**

**Photo 24**

Finish the main ring seal. Adjust the o.d. of the 35mm emerging from the apparatus (Photo 24). Round off the vacuum jacket, attach a 3/8" tube at the end, and prepare it for evacuation and tipping off (Photos 25 & 26).

**Photo 25**

**Photo 26**

**Photo 27**

Seal the water jacket opening nearest the main ring seal and open it up for the hose connector (Photo 27). Remove some material from the end of the hose connector *180 degrees* from the scratch made earlier. This will prevent too much material on the inside of the tangential sidearm. Attach the hose connector assuring the alignment with the other features of the spray chamber (same side as support rods, 90 degrees from drain, etc.) (Photo 28). Next, attach the 1/4" medium wall tube to the top of the discard portion of the hose connector and attach the previously folded latex hose to it (Photo 29).

**Photo 28**

**Photo 29**

**Photo 30**

Seal the second water jacket opening and open it for the next hose connector (Photo 30). On this connector, remove extra material at the opening on the *same* side as the scratch. Attach the connector making it parallel with the other (Photo 31). Remove the

**Photo 31**

blow hose from the 1/4" and stow it back under the rubber band. Remove the 1/4" tube. Turn the piece over to point the connectors down, break off both hose connector tubes, and firepolish the ends (Photo 32).

**Photo 32**

**Photo 33**

Seal down on the drain opening (Photo 33). At the same moment the glass seals on the opening, remove the cork from the 3/8" vacuum jacket tube. Turn the chamber over, placing the seal on the underside, and finish it. Open it up for the large hose connector drain. Attach the drain at a slight angle away from the main ring seal (Photo 34).

**Photo 34**

Open up the small seal near the main ring seal and attach a 12/5 socket, 20mm long, angling back and in pointing toward the end of the nozzle (Photos 35, 36 & 37). This should point it at the radius center of the three rounded tubes. With a hot flame, go over the outer jacket very well to flame away any strain line deposits (Photo 38). The silvering of the vessel will show up any marks formed by strain. Place into a hot furnace and anneal.

**Photo 35**

**Photo 36**

**Photo 37**

**Photo 38**

**Photo 39**

Trim all the ends and firepolish all but the 35mm which is chamfered (Photo 39). Silver the vessel, evacuate to 10 -1 TORR, and tip off the vacuum line (Photo 40). This finishes the spray chamber.

**Photo 40**

# Technical Posters 2000

**Peter Hatch – "Replacing Broken Cobalt Glass Inserts for Antique Dining Set"**
University of Iowa
Chemistry Department, 161CB
Iowa City, IA 52242
(319) 335-1337
Peter-hatch@uiowa.edu

**Doni Hatz – "Double Manifold"**
Proctor and Gamble Company
Miami Valley Labs
P.O. Box 538707
Loveland, OH 45140
(513) 627-2313
hatzdj@pg.com

**James R. Hodgson – "Nomenclature for Scientific Glassblowers"**
Kansas State University
Department of Chemistry
111 Willard Hall
Manhattan, KS 66506
(785) 532-6676
Hodgson@ksu.edu

**Carl Nyman – "What to Do with Old Bottles – Wine and Beer"**
Sulphides Revisited
18280 S. W. Butternut Street
Aloha, OR 97007
(503) 649-3327

**Kevin Teaford – "One-Step Ring Seal Sidearm"**
Precision Glassblowing of Colorado, U.S.A.
14775 East Hinsdale Avenue
Englewood, CO 80112
(303) 693-7329
preglass@unidial.com

# Technical Workshops 2000

Scott Bankroff – *Michigan State University*
**"Fusing Round Optical Windows to Square Tubing"**

Gary Coyne – *California State University L.A.*
**"Wooden Fixtures for Schlenk Line Construction"**

Doug DeWitt – *Perkin Elmer/ILC Technologies*
**"Camera Measuring"**

Julie Ellington – *Clear Concepts*
**"Fluorescent Cells"**

Eric Hauser – *Farlow's Scientific Glassblowing, Inc.*
**"Using Litton Drag Bar Tooling"**

Skip Huckaby – *Orca Glaswerke, Inc.*
**"Frit Sealing Techniques"**

Wade Martindale – *Farlow's Scientific Glassblowing, Inc.*
**"Heart Model"**

Darren McGinnis – *Farlow's Scientific Glassblowing, Inc.*
**"Quartz Pyrol Tube"**

Mike Souza – *Princeton University*
**"Constructing User-Friendly Vacuum Manifolds"**

Kevin Teaford – *Precision Glassblowing of Colorado*
**"One-Step Double Ring Seal Sidearm"**

The video versions of these Technical Workshops are in the ASGS video library and are available to be loaned out.

# 2000 Exhibitors

**American Laboratory Supply**
1033 Ohio Ave.
Richmond, CA 94803
510-620-0220

**Andrews Glass Co.**
3740 NW Blvd.
Vineland, NJ 08360
856-692-4435

**Blue Flame Technology**
431 Kentucky Lane
McKinney, TX 75069
972-542-2571

**Carlisle Machine Works Inc.**
PO Box 746
Building 68 Municipal Airport
Millville, NJ 08332
800-922-1167

**Chemglass Inc.**
3861 N. Mill Road
Vineland, NJ 08360
800-843-1794

**Corning Inc.**
PO Box 5000
Corning, NY 14830
607-974-0350

**Friedrich & Dimmock, Inc.**
PO Box 230
Millville, NJ 08332
800-524-1131

**G-Tec Natural Gas Systems**
401-William L. Gaiter Parkway
Buffalo, NY 14215
800-451-8294

**Glass Warehouse**
PO Box 1039
800 Orange St.
Millville, NJ 08332
609-327-5228

**GM Associates Inc.**
9824 Kitty Lane
Oakland, CA 94603
510-430-0806

**Heathway Inc.**
4030 Skyron Drive #C
Doylestown, PA 18901-1135
215-348-2881

**J. Young Scientific Glassware LTD**
11 Colville Road
Acton, London W38BS
UK
44-20-8992-0891

**Kimble/Kontes Glass Co.**
PO Box 1502
Vineland, NJ 08362
888-546-2531

**Larson Electronic Glass Inc.**
2840 Bay Rd.
PO Box 371
Redwood City, CA 94064
650-369-6734

**Litton Engineering Labs**
Suite 200 Litton Drive
Grass Valley, CA 95945
800-821-8866

**M-Tech Industries/ B & C Machine**
PO Box 1358
Cedar Ridge, CA 95924
530-273-6176

**Miema**
28 Rue de Thys
Oreye 4360
Belgium

**Mindrum Precision**
10,000 4th St.
Rancho Cucamonga, CA 91730
909-989-1729

**National Diamond Lab**
4650 Alger St.
Los Angeles, CA 90039
800-898-8665

**North Jersey Diamond Wheel**
218 Little Falls Road
Cedar Grove, NJ 07009
800-822-3341

**Pedco-Hill Inc.**
91 Steamwhistle Drive
Ivyland, PA 18974
215-942-5193

**Pegasus Industrial Specialties Inc.**
530 Masey Rd.
Guelph, ONT N1K 1B4
Canada
800-315-0387

**Schott Corporation**
3 Odell Plaza
Tech Glass Division
Yonkers, NY 10701
914-968-8900

**VM Glass Co.**
3231 N. Mill Road
Vineland, NJ 08360
856-794-9333

**Wale Apparatus Co. Inc.**
PO Box D
Hellertown, PA 18055-0201
800-334-WALE

**Wilmad-Labglass Co.**
PO Box 688
Buena, NJ 08010-0688
800-220-5171 x652

**Wilt Industries Inc.**
Rte. 8
Lake Pleasant, NY 12108
800-232-9458

# 45th Symposium Attendees

Juergen Achatz
Sean Adams
Tom Adams
Charles Amling
Jane Anderson
Jeffrey Anderson
Steven Anderson
Mark Andrews
Arthur Arias
Michael Arias
Jörgen Averlino
J. Jeffrey Babbitt
Ruth Babbitt
Joel Babbitt
Maisy Babbitt
Chuck Bakus
Ron Banes
Terry Banes
Scott Bankroff
Debra Begg
Thomas Biebel
Ronald Bihler
Kenneth Bittner
Nancy Bittner
Guenther Boepple
Eileen Bolan
Theodore Bolan
Ron Bolnick
William Bourbeau
James Breen
Ken Brick
Linda Brick
Ben Brown
Allan Brown
Corey Brown
Marylin Brown
Tyrone Brown
Daniel Brucker
Larry Burkhardt
Bill Butek
Tish Buti
Wayne Buti
James Byrnes
Deborah Camp
Phil Carey
Carolyn Chabot
John Chabot
Larry Circosta
Bonnie Clark
Brenda Cloninger
Jerry Cloninger
Ann Coe
Patti Combes
Bob Concannon
James Cornell
Laura Cornell
LuAnn Cossaboon
Dennis Courtney
Gary Coyne
David Daenzer
John Dami
Margaret Decoux
Paul Decoux
Patrick Feflorio
Gary Delkamp
Tom Denton
Douglas Dewitt
Darcey Doering
Elaine Doering
Ann Dougherty
Diane Draper
Dr. Clifton Draper
Jay Draper
Ruth Dykstra
Alexandria Edwards
Daniel Edwards
Danielle Edwards
Diane Edwards
Lisa Edwards
Nicole Edwards
Gary Farlow
Nathan Fligge
Trond Forre
Carolyn Forrester
Jill Fox
Jon Fox
John French
John Fuller
Mitzie Fuller
Bill Furney
Teri Gabbard
Glenn Gados
Victor Gallicchio, Jr.
Robert Gant
Antonia Garcia
Alberta Gerhart
Richard Gerhart
Sue Gettinger
Georg Glaser
Bill Godfrey
Robert Goffredi
Sharon Goffredi
Ruth Gowell
Rafel Grandos
Robert Greer
Joseph Gregar
Katie Gregar
Gary Gregston
Michael Greico
Steve Grimm
Chander Grover
Sumi Grover
Adolf Gunther
Bradley Guth
Tad Haas
Nancy Hagmaier
Robert Halbreiner
Kim Haleck
Arthur Hanner
Randall Hansen
Andre Hardenne
Don Harris
Tom Hassur
Lois Hatch
Peter Hatch
David Hatz
Doni Hatz
Howard Hayman
Peter Hazlett
Frank Hedges
Paul Henrickson
Amy Henthorne

Timothy Henthorne
Hiroko Herbert
Volker Herbert
Cas Hernandez
Jeanne Hill
Newton Hill
Newt Hill, Jr.
Ed Hioki
Jeff Hocevar
Dawn Hodgkins
Donald Hodgkins
James Hodgson
C. David Hopkins
Gwen Hopkins
John Hopkins
Ed Howard
Jerry Howard
Thomas Howe
Tollie Howe
Kendal Hunt
Lynn Husbands
Mark Husbands
Joseph Izzo
Patricia Izzo
Ralph Joiner
Kevin Keller
Sharon Kelly
Aretha Ketch
Robert Ketch
Craig Kloss
Gary Koopman
Jack Korfhage
Charlie Kornahrens
Sue Kornahrens
Timothy Kornahrens
Andrew Kousmine
Kristine Kousmine
Laura Kousmine
Marc Kousmine
Mike Kousmine
Charles Kraft
Jan Kraft
Jill Kraft-Santa
Keith Krumnow
JoAnn Kuehl
Keith Kuehl
Egon Kummer
Fridolin Kummer
Hedi Kummer
Sonja Kummer
Janice Kyle
Steven Kyle
Mary L'Abbe
Peter L'Abbe
Barry Lafler
Devin Lafler
Gordon Lafler
Andrew LaGrotte
Jeff Lakeman
Susan Lane
Mikael Larsson
Cindi LeBaron
Rand LeBaron
Andrew Ledden
Jean-Marc Lefebvre
L. Frederick Leslie
Matt Leslie
Meryl Leslie
Bonnie Lew
Morris Lew
Robert Lewandowski
Clement Lim
Janeille Litton
Michelle Litton
Charles Litton, Jr.
Dennis Longnecker
Mike Lozanoff
Klaus Lursch
Richard Mack
Chuck Martin
Stephanie Martin
Susan Martin
Timothy Martin
Wayne Martin
Wade Martindale
Wilbur Mateyka
Pat Mathews
Victor Mathews
Darren McGinnis
Bill McLaughlin
Elaine Meints
Frank Meints
John Melvin
William Merka
James Merritt
Sharon Merritt
Deborah Miller
Dan Mindrum
Hedy Misch
Manfred Misch
Steven Dean Moder
Arleen Molodow
Marvin Molodow
Diane Morphew
Joseph Morphew
Joseph Morphew, Sr.
Diann Morris
Michael Morris
Rita Morris
Roxanne Morris
Danny Murphy
Thomas Murphy
T. Thomas Nagami
Anthony Gene Nelson
Lori Neu
Peggy Nichols
Robert Nichols
Jeff Noyes
Jennifer Noyes
Diane Nutter
Mel Nutter
Carl Nyman
Rose Nyman
Tim O'Brien
Dan O'Grady
Sarah Ohmann
Thomas Orr
Kenneth Owens
Michael Palme
Angie Parillo
Edward Parillo
Amamda Partlow
Jennifer Partlow
Joseph Partlow
Mary Partlow
Greg Pfalmer
Pam Pfalmer
John Pirolo

Monica Pirolo
Joe Plumbo
John Plumbo
Lynnette Ponton
Melissa Ponton
Richard Ponton
Robert Ponton
Edwin Powell
Brian Powers
Stacy Powers
Sally Prasch
Cheryl Reichard
Dave Reichard
Kathryn Renshaw
Heriberto Rivera
Bill Roach
Donna Roach
Monty Roach
Mark Robel
Christine Roeger
Jim Roeger
Arno Roensch II
Hans Rohner
Michael Ronalter
Gerhard Rossbach
Steve Russo
William Sales
Douglas Schade
Bob Schlher
Maria Schlott
Rudolf Schlott
Brian Schwandt
A. Ben Seal
Joan Seal
David Searle
Bobbie Seatrunk
Chris Shave
Terry Shidner
Robert Singer
Jan Singhass
Ron Sjolander
Sharon Skenandore
Laura Sliwoski
Mersades Sliwoski
Phillip Sliwoski
David Smart
Katie Smart
Gordon Smith
Linda Smith
Richard Smith
Patrick Smythe
Marie Snodgrass
Robert Snodgrass
Michael Souza
Joane Speakman
William Spencer
Christopher Sprague
Jayne Sprague
Sarah Staton
Thomas Stefanek
Dennis Steffey
Parker Stowman
Sarah Stowman
Bruce Suba
Bryce Suba
Karlee Suba
Kathy Suba
David Surdam
Phil Surdam
Walt Surdam
Kevin Teaford
Stefau Teungstrom
Mark Toonen
Jaun Torres
Brad Trego
Sarah Trego
Kathy Trent
Mary Trent
Neal Trent
Ron Trent
Lisa Vanegas
Winnie Vierra
Robert Waddington
Robert Wallace
Andrew Wargo
Dennis Wargo
Pat Wargo
Conrad Warren
David Wedsworth
Peter Werner
Dave Werth
Michael Werth
Tracy Werth
Lanah Wheeler
Michael Wheeler
John Whelan
Mark Wicker
Randolph Wilkin
Daniel Wilt
Donald Woodyard
Glenna Yee
Damon Young
Jay Zahran
Oliver Zavoda